



Sub-slab mantle anisotropy beneath south-central Chile

Stephen P. Hicks*, Stuart E.J. Nippres, Andreas Rietbrock

School of Environmental Sciences, University of Liverpool, Liverpool L69 3GP, UK

ARTICLE INFO

Article history:

Received 9 May 2012

Received in revised form

8 September 2012

Accepted 15 September 2012

Editor: P. Shearer

Available online 23 October 2012

Keywords:

south-central Chile

subduction

shear-wave splitting

seismic anisotropy

mantle flow

asthenospheric entrainment

ABSTRACT

Knowledge of mantle flow in convergent margins is crucial to unravelling both the contemporary geodynamics and the past evolution of subduction zones. By analysing shear-wave splitting in both teleseismic and local arrivals, we can determine the relative contribution from different parts of the subduction zone to the total observed SKS splitting, providing us with a depth constraint on anisotropy. We use this methodology to determine the location, orientation and strength of seismic anisotropy in the south-central Chile subduction zone. Data come from the TIPTEQ network, deployed on the forearc during 2004–2005. We obtain 110 teleseismic SKS and 116 local good-quality shear-wave splitting measurements. SKS average delay times are 1.3 s and local S delay times are only 0.2 s. Weak shear-wave splitting from local phases is consistent with a shape preferred orientation (SPO) source in the upper crust. We infer that the bulk of shear-wave splitting is sourced either within or below the subducting Nazca slab. SKS splitting measurements exhibit an average north-easterly fast direction, with a strong degree of variation. Further investigation suggests a relationship between the measurement's fast direction and the incoming ray's back-azimuth. Finite-element geodynamic modelling is used to investigate the strain rate field and predicted LPO characteristics in the subduction zone. These models highlight a thick region of high strain rate and strong S-wave anisotropy, with plunging olivine *a*-axes, in the sub-slab asthenosphere. We forward model the sub-slab sourced splitting with a strongly anisotropic layer of thick asthenosphere, comprising an olivine *a*-axis oriented parallel to the direction of subduction. The subducting lithosphere is not thick enough to cause 1.2 s of splitting, therefore our results and subsequent models show that the Nazca slab is entraining the underlying asthenosphere; its flow causes it to be strongly anisotropic. Our observation has important implications for the controlling factors on sub-slab mantle flow and the movement of asthenospheric material within the Earth.

© 2012 Elsevier B.V. All rights reserved.

1. Introduction

Many geodynamic processes in the Earth's subsurface leave behind a signature of seismic anisotropy; this is the dependence of a seismic wave's propagation direction on its velocity. Shear-wave splitting analysis is one of the most robust and popular methods of inferring seismic anisotropy. Shear-wave splitting occurs when a single S-wave passing through an anisotropic medium splits into a fast component and a delayed slow component. A splitting measurement is characterised by two parameters: fast polarisation direction (hereafter, fast direction) and the difference in arrival times between fast and slow components (hereafter, delay time). It is analogous to the optical birefringence seen in anisotropic materials under polarised light. The fast direction indicates the geometry of anisotropy within the medium; the delay time indicates both the strength of seismic anisotropy and the anisotropic layer's

thickness. Shear-wave splitting can resolve lateral variations in seismic anisotropy; however, its depth resolution is poor, resulting in the inherent non-uniqueness of interpretations.

Due to the complex geodynamics associated with subduction zones, there have been numerous shear-wave splitting studies (e.g. Long and van der Hilst, 2006; Hammond et al., 2010) over the last two decades focused on determining the anisotropic structure of these margins. The overriding lithosphere, the supra-slab asthenosphere, the sub-slab asthenosphere and the subducting oceanic lithosphere have all been proposed to contain sources of seismic anisotropy. With these numerous sources, along-strike variations in subduction characteristics and the poor depth resolution inherent in shear-wave splitting, there is no one model which fits all global subduction zone splitting observations. It is possible to reduce the depth uncertainty by analysing splitting in both teleseismic SKS arrivals and local S-waves emanating from the slab. Predicting the spatial variation in seismic anisotropy through numerical geodynamic modelling (e.g. Fischer et al., 2000; Kneller and Van Keken, 2007) can also help to further localise potential sources.

* Corresponding author. Tel.: +44 151 794 5160.
E-mail address: s.hicks@liv.ac.uk (S.P. Hicks).

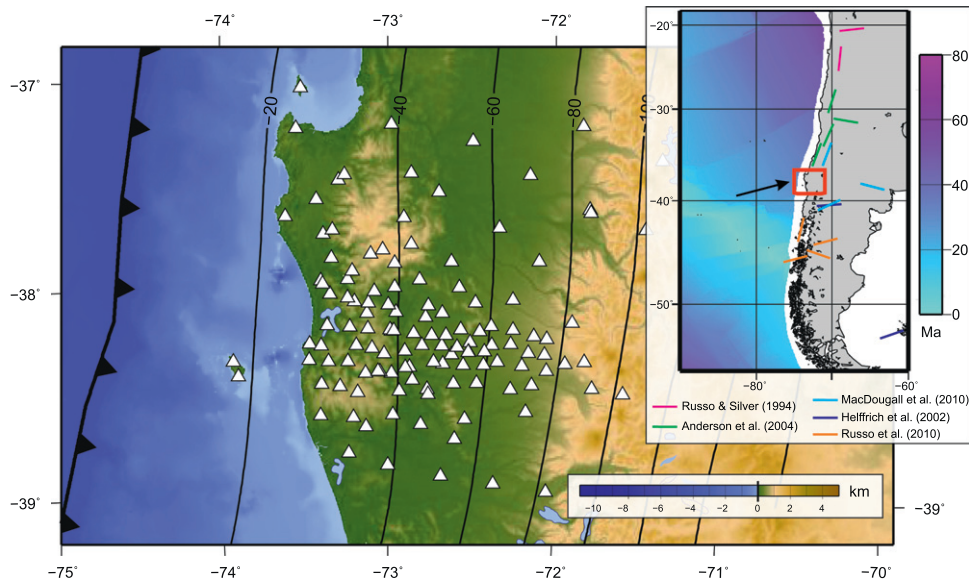


Fig. 1. Map of the south-central Chile forearc region. The inset map shows the location of the study area (red box) in relation to the western margin of South America, and describes the overall pattern of teleseismic fast direction from the previous studies of seismic anisotropy in the region. The age of oceanic Nazca plate offshore of this margin is illustrated. The black arrow indicates the convergence direction of the Nazca plate relative to the South American plate. On the main map, TIPTEQ stations used in this study are denoted by the white triangles. Black lines give the depth in km to the top of the downgoing Nazca slab (Hayes and Wald, 2009). The scale bar at the bottom-right is for bathymetry/topography. (For interpretation of the references to color in this figure caption, the reader is referred to the web version of this article.)

Both sub-slab and supra-slab asthenospheric flows are likely the biggest contributors to splitting due to the lattice preferred orientation (LPO) of olivine under shear (e.g. Mainprice et al., 2005). Anisotropy caused by supra-slab asthenospheric flow is well studied in a number of subduction zones; it appears to be affected by 3D slab geometry (e.g. Polet et al., 2000; Peyton et al., 2001; Anderson et al., 2006; Kneller and van Keken, 2008), and the presence of melt, water, and olivine fabric transitions (e.g. Karato et al., 2008), but remains poorly constrained. Sub-slab sourced anisotropy, however, is less well studied. Most subduction zones are inferred to comprise trench-parallel, asthenospheric flow beneath the slab, due to slab-rollback induced barrier flow (Long and Silver, 2009). There are several exceptions to this rule; one example is Cascadia, where observations of trench-perpendicular splitting are believed to be caused by a thick sub-slab decoupling zone (Long and Silver, 2009) with entrainment of the underlying asthenosphere in the direction of the slab's absolute plate motion (APM). Furthermore, Hammond et al. (2010) suggest that the oceanic mantle in the Sumatran subduction zone contains anisotropy in the direction of the plate's APM caused by development of LPO, and its subsequent preservation, during formation of lithosphere at spreading centres.

Seismic anisotropy also develops through shape-preferred orientation (SPO) in aligned faults, fractures and melt inclusions. Shear-wave splitting caused by SPOs in the crust is believed to result in regional fast directions parallel to the maximum horizontal compressive stress direction, σ_H (Crampin et al., 2004), and locally, parallel to the strike of major faults (Ozalaybey and Savage, 1995). Recent work by Faccenda et al. (2008) and Healy et al. (2009) suggests that deep-seated normal faults in the subducting oceanic lithosphere could be a significant contributor to trench-parallel shear-wave splitting, although the strength of anisotropy is dependent on the volume fraction of antigorite-filled fractures and their aspect ratio (Faccenda et al., 2008).

The traditional first-order pattern of SKS splitting along the Andean margin is strong splitting (delay times of 1–2 s) with trench-parallel fast directions (e.g. Russo and Silver, 1994; Rokosky et al., 2006; Long and Silver, 2008), caused by sub-slab asthenospheric barrier flow (Long and Silver, 2009). With recent shear-wave splitting observations from dense seismic networks

(e.g. Polet et al., 2000; Anderson et al., 2006), however, this picture appears to be looking more complex (Fig. 1, inset). These studies reveal the existence of several significant rotations to trench-perpendicular flow; one such example is in central Chile, where changes in slab geometry are thought to initiate complex three-dimensional flow (Anderson et al., 2006). Another region of interest is the Chile ridge triple-junction in southern Chile, where a sharp southerly transition from trench-parallel flow to trench-perpendicular flow is suggested to be caused by sub-crustal derived asthenosphere flowing into the Patagonian slab window (Russo et al., 2010). In south-central Chile, Helffrich et al. (2002) and MacDougall et al. (2010) analysed shear-wave splitting data from a permanent station, PLCA, located at 40°S. Helffrich et al. (2002) observed strong teleseismic shear-wave splitting parallel to the direction of the South American plate's APM, and attributed this to mantle flow driven by both Atlantic plume buoyancy flux and Nazca slab rollback. MacDougall et al. (2010) reveal that strong teleseismic delay times continue further east, at station TRQA, located in the back-arc, although the fast polarisation directions become more ENE oriented. They also observed relatively strong (< 0.9 s) local splitting at both stations; this is evidence for supra-slab asthenospheric flow.

In this study, we use data from a dense temporary seismic array concentrated on the south-central Chilean forearc in order to test models of anisotropic sources both within, and beneath, the slab. The uniform slab geometry beneath the region allows us to interpret sub-slab asthenospheric flow without the complicating factor of three-dimensional mantle flow. We present shear-wave splitting measurements and numerical models to support a new mechanism of seismic anisotropy in this region along the Andean margin, which involves sub-slab entrained asthenospheric flow.

2. Geotectonic setting

The Andean margin of South America is characterised by convergence between the oceanic Nazca plate and the continental South American plate; this is accommodated by the slightly oblique subduction of the Nazca plate beneath the overriding

South American plate, at the Chile trench (Fig. 1). In this paper, we focus on the south-central Chile forearc at around 38°S; here the 30 Ma Nazca plate (e.g. Tebbens and Cande, 1997; Müller et al., 2008) converges with South America at a rate of approximately 66 mm yr⁻¹ (e.g. Angermann et al., 1999; Gripp and Gordon, 2002). Wadati-Benioff seismicity indicates a shallow dipping (30°) slab beneath the forearc, with the deepest seismicity at 115 km depth (Bohm et al., 2002; Haberland et al., 2006, 2009). The oceanic Moho has been imaged at both the outer-rise and beneath the forearc, suggesting an oceanic crustal thickness of 8 km (Contreras-Reyes et al., 2007; Groß and Micksch, 2008). Offshore of the trench, deep-seated normal faults have been observed, and are believed to continue in the subducted crust, landward of the trench (Contreras-Reyes et al., 2007).

The geometry of the subducting Nazca slab interface and the overriding continental lithospheric structure are well understood in this region following the three-dimensional velocity model of Haberland et al. (2009). The overriding continental forearc reaches a maximum depth of ~50 km beneath the Coastal Cordillera, ~200 km from the trench. This coincides with the furthest westward extent of continental mantle and the downdip limit of the seismogenic zone. Beneath the forearc basin, ~230 km from the trench, the continental crust is significantly thinned to 30 km. Supra-slab asthenospheric mantle is not believed to be present beneath the study region. A prominent feature of the continental crust is the steeply dipping, northwest-striking Lanalhue fault zone; it has been imaged to 10 km depth (Groß and Micksch, 2008) and is related to localised intra-plate seismicity (Haberland et al., 2006). It is predominately a sinistral strike-slip fault, which is associated with several secondary fault splays. Melnick et al. (2009) speculate that this fault zone could extend through the entire crust, interacting with the seismogenic zone at the subduction interface.

3. Data and method

The TIPTEQ (The Incoming Plate to Megathrust Earthquake Processes) project deployed a temporary seismic array between November 2004 and October 2005 in south-central Chile (Rietbrock et al., 2005; Haberland et al., 2006, 2009). The array covered the entire forearc over an area of approximately 250 km² (Fig. 1); it comprises of 120 stations equipped with three-component short-period seismometers. The dense station spacing (less than 5 km in places) and numerous high quality local S-wave arrivals permit a high resolution study of the anisotropic structure beneath this region.

In total, we analyse 219 teleseismic events within the SKS epicentral distance range, corresponding to ~7400 SKS waveforms. Most events were sourced in the Tonga–Kermadec, Indonesian and Philippine subduction zones. For local events, we use the catalogue of Haberland et al. (2009), which contains 439 relocated local earthquakes. In total, we use 30 local events located beneath the central valley and the western margin of the volcanic region to ensure that source-receiver angles fall within the shear-wave window. Most events were located at either the upper plate interface of, or within, the subducting oceanic crust. Several events were located within the overriding continental crust.

Prior to shear-wave splitting analysis, we bandpass filter the teleseismic and local seismic traces in the frequency ranges 0.01–0.30 Hz and 0.10–1.00 Hz, respectively. The overlap in these frequency ranges ensures that differential frequency dependent effects on splitting results are minimised to ensure a coherent interpretation (Hammond et al., 2010).

For the shear-wave splitting analysis, we use the method of Silver and Chan (1991), which corrects the split elliptical S-wave back to linear particle motion. The algorithm does this by performing a grid search over all possible values of fast polarisation, ϕ and delay time,

δt . For a given time window, the most stable combination of these is the one which minimises the second eigenvalue of the particle motion covariance matrix. We employ the Teanby et al. (2004) algorithm to semi-automatically perform the grid search on a number of window lengths, using cluster analysis to ensure that a splitting measurement is stable over many different windows. This method automatically calculates the source polarisation direction during the splitting calculation.

A measurement is defined as “good” if the splitting measurement analysis has a signal to noise ratio, $\text{SNR} \geq 3$ (Restivo and Helffrich, 1999), the particle motion becomes linearised with minimisation of energy on the transverse component after correction. During the cluster analysis stage, we look for a tight group of clusters to ensure that the measurement is not sensitive to window length. Furthermore, for the SKS splitting, the source polarisation direction (SPOL) should be approximately equal to the ray’s theoretical back-azimuth (BAZ) due to the radial polarisation at the core-mantle boundary (e.g. Hammond et al., 2010). Measurements which yield a SPOL-BAZ residual greater than $\pm 30^\circ$ are rejected. Good measurements also have 1σ errors less than $\pm 10^\circ$ in fast direction (ϕ), and ± 0.3 s in delay time (δt). Linear particle motion on the original rotated traces are diagnostic of a null measurement; these are not included in the final analysis. See Figs. S1 and S2 for an example of good quality SKS and local S splitting measurement, respectively.

4. Results

4.1. Teleseismic SKS splitting results

We obtain a total of 110 good quality SKS splitting measurements (Fig. 2a). The average fast direction is NE, although there is variability about this direction. This average fast direction does not fall into the traditional trench-parallel or trench-perpendicular fast direction classification, but rather trench-oblique. There is also clear intra-station variability in fast directions of up to 30°. There appears to be no spatial trend in fast direction. Delay times are also variable, ranging from 1.0 to 1.9 s, with an average of 1.3 s. Measurements taken offshore, on Isla Mocha, have the same fast direction trend, but have a smaller average delay time of 1.1 s; this is 0.2 s less than the network’s average. We find that there is no dependence of the splitting parameters on the window length used for the splitting analysis (Fig. S3).

We find a clear variation of fast direction with back-azimuth across the network (Fig. 2a): the two main back-azimuths, west and south, tend to correspond to ENE and NNE fast directions, respectively. For the other back-azimuths, we also observe a correlation with fast direction. By stacking the measurements by back-azimuth (Restivo and Helffrich, 1999), we obtain coherent resultant stacks, so this apparent relationship is not simply an artefact of poorly defined confidence limits in ϕ – δt space. We do not, however, find such a clear correlation of delay time with back-azimuth (Fig. S4). Examples of good quality splitting measurements from each of the two main back-azimuths at station N410 are illustrated in Figs. S5 and S6.

We use TauP_Pierce (Crotwell et al., 1999) to calculate the raypaths for each SKS splitting measurement by raytracing through the reference velocity model, AK135 (Kennett et al., 1995) (Fig. 2b). Many rays have sub-vertical incidence angles of ~15° in the sub-slab asthenosphere. The two main back-azimuthal clusters have different raypaths at depth, but begin to converge and sample the same material at about 250 km depth.

4.2. Local S splitting results

Local splitting measurements were analysed on S-waves generated by earthquakes at 20–95 km depth, with incidence angles within

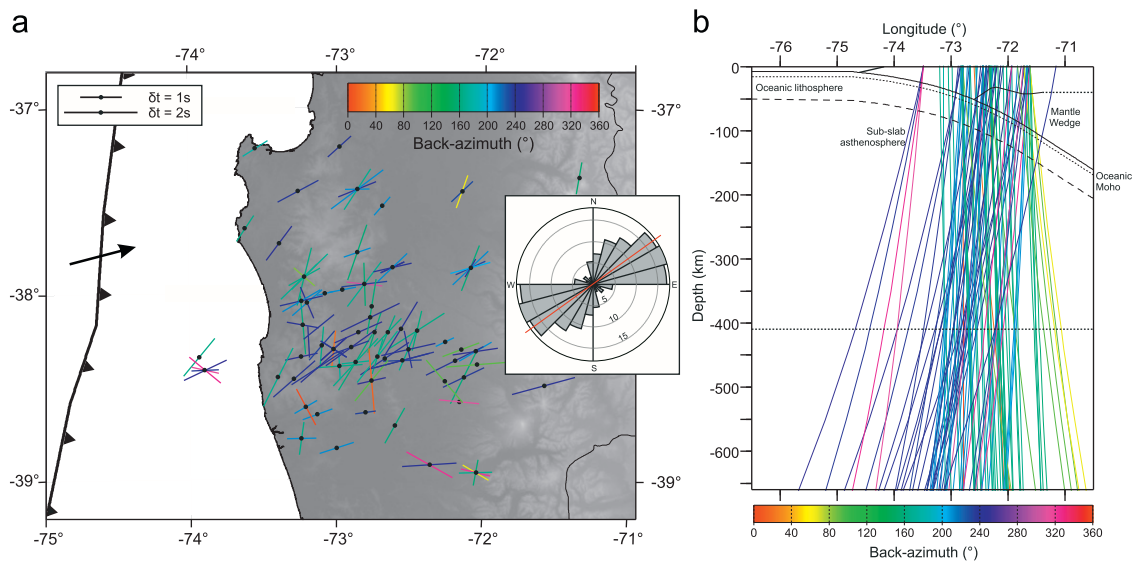


Fig. 2. (a) Map of all good teleseismic (SKS) splitting results, plotted at the corresponding station location. The orientation and length of the bar reflect the fast direction and delay time, respectively. The bars are coloured by the back-azimuth of the ray for each measurement. The black arrow indicates the convergence direction of the Nazca plate relative to the South American plate. Inset: bi-directional rose diagram for all these measurements, in bins of 15°, with the red line representing the mean fast direction. (b) SKS ray geometries in the upper mantle and lithosphere. Raypaths are projected onto a west–east vertical section. Distinct subduction domains are shown. The upper slab interface is from Hayes and Wald (2009), the continental Moho from Haberland et al. (2009), the oceanic crust is 8 km thick based upon Contreras-Reyes et al. (2007). The raypaths start to sample the same material from about 250 km depth. (For interpretation of the references to color in this figure caption, the reader is referred to the web version of this article.)

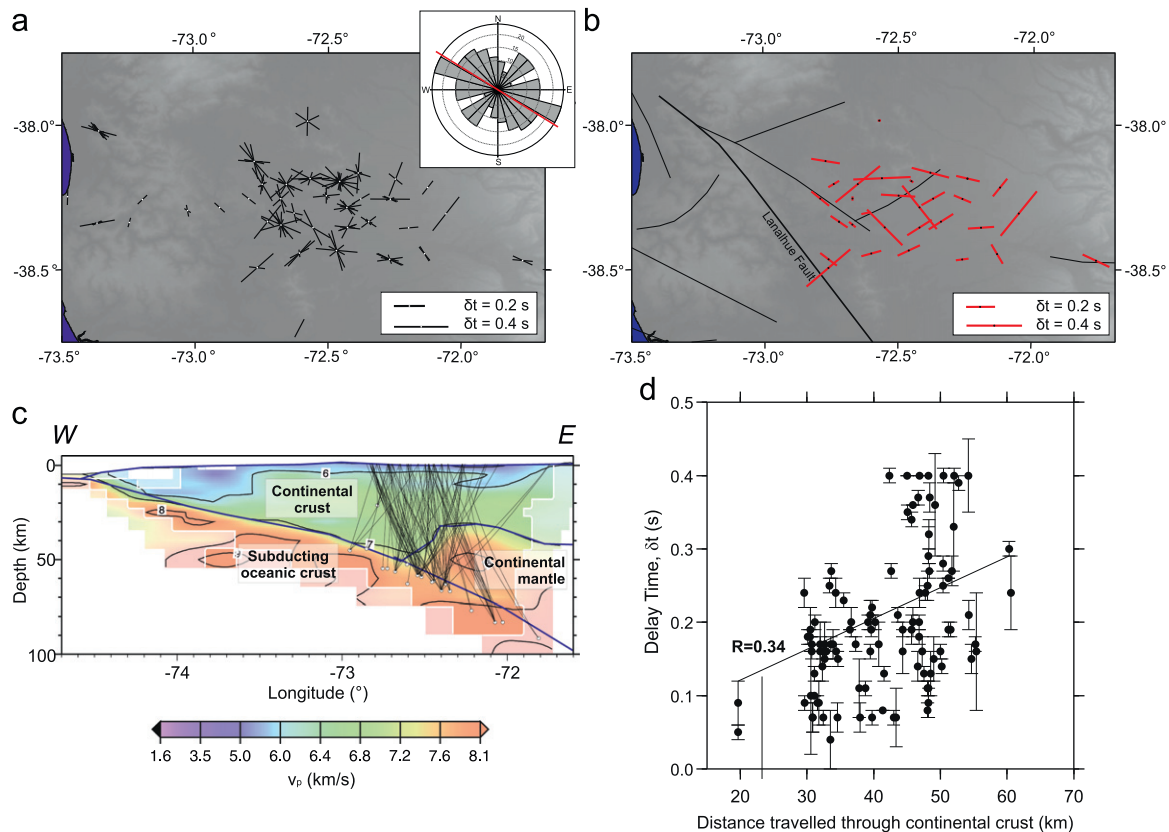


Fig. 3. (a) Individual local S splitting measurements, plotted at the corresponding station location. Inset: Bi-directional rose diagram of fast directions from the good local splitting measurements, plotted in bins of 15°. (b) Station-stacked splitting measurements, plotted at the corresponding station location. Black lines indicate crustal faults after Melnick and Echtler (2006). (c) Local S raypaths. For illustration purposes, the background colour is the 2D P-wave velocity model for this region of Haberland et al. (2009). The black lines are the raypaths for which good splitting measurements are obtained. Black circles represent the hypocentre locations. (d) Delay time as a function of distance travelled by each ray through the continental crust. The correlation coefficient, R is shown. Error bars represent 1 σ error in δt .

the shear-wave window. From 235 waveforms, we obtain 116 good quality splitting measurements. Fast directions are variable; their mean fast direction is close to ESE, trench-oblique (Fig. 3a). Delay

times are all less than 0.4 s with an average of 0.2 s. There is no clear spatial variability. Most stations where we have stable shear-wave splitting measurements are located within the central valley basin.

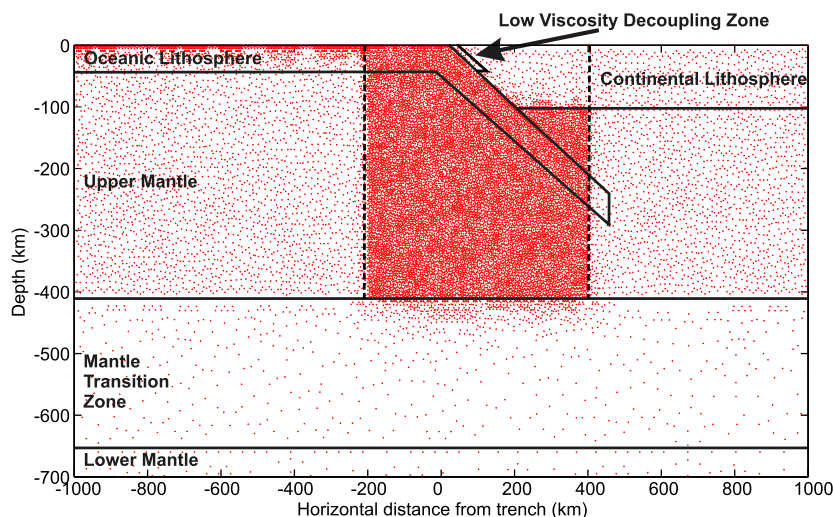


Fig. 4. 2D finite element modelling set-up showing the scheme of parameterisation into the various subduction zone domains. Red points give the nodal locations in the model. The upper mantle and lithospheric regions are laterally subdivided to give a dense nodal spacing around the subducting lithosphere. (For interpretation of the references to color in this figure caption, the reader is referred to the web version of this article.)

Source and station stacks were calculated using the algorithm of Restivo and Helffrich (1999), an adaptation of the method proposed by Wolfe and Silver (1998). Station stacking produces the most coherent result; it gives consistent alignment of fast directions across the network and results in the best constrained stack in ϕ – δt space. We also find that fast directions from our station stacks may align with the orientation of mapped crustal faults (Fig. 3). A number of these stations are located close to the Lanahue fault zone and some of its subsidiary splays. We observe no relationship between the splitting parameters and either source polarisation direction or the focal depth of the earthquakes.

We investigate the possibility of path-length dependent delay times; a relationship would be expected if all the regions that the rays travel through had consistent fast directions. We calculate the raypaths of good local shear-wave splitting measurements using the high resolution 3-D S-wave velocity model of Haberland et al. (2009). We parameterise the region into three major subduction zone domains: the continental crust, the continental mantle and the subducting oceanic lithosphere (Fig. 3c). The parameterisation is based on the two-dimensional velocity model, since along-strike changes have been shown to be minimal (Haberland et al., 2009).

Fig. 3c shows the rays projected onto a W–E section, plotted on top of the two-dimensional parameterised structure. Some rays travelled from the slab through the continental crust, without interaction with the lithospheric mantle.

A weak positive correlation ($R=0.34$) between the path length through continental crust and delay time is observed (Fig. 3d), suggesting that most of the local shear-wave splitting is generated in the overriding South American crust, but the small correlation coefficient indicates a highly heterogeneous crust. We find no correlation between path lengths through the continental mantle or oceanic crust with delay time. This leads us to believe that these regions contribute minimally to the total observed splitting delay time.

5. Modelling

5.1. Geodynamic modelling

In order to determine which subduction zone domains (e.g. continental lithosphere, oceanic lithosphere, asthenosphere, etc.)

are candidates to contain the main source of SKS splitting, we aim to produce numerical geodynamic models of the south-central Chilean subduction zone. In this region, the direction of subduction is almost perpendicular to the trench, so we can use a two-dimensional model oriented parallel to the direction of subduction. We use MILAMIN (Dabrowski et al., 2008), a two-dimensional thermo-viscous modelling algorithm, which uses coupled finite element and mechanical solvers (Fry et al., 2009) to model the temperature, velocity and strain rate fields in the subduction zone. We parameterise the model space into several subduction zone domains: oceanic lithosphere, continental lithosphere, a low viscosity decoupling zone, upper mantle, mantle transition zone and lower mantle (Fig. 4). A non-uniform nodal spacing is used to ensure high resolution around the subducting lithosphere. We use a minimum nodal spacing of 5 km in this high resolution area (e.g. Richardson and Coblenz, 1994) and a maximum nodal spacing of 50 km in the lower mantle. Prior to subduction, the temperature of the upper mantle is set at 1200 °C. We impose the following mechanical boundary conditions: zero vertical velocity at the top (0 km depth) and at the bottom (1000 km depth) of the model, and zero horizontal movement at the top of the overriding plate, which acts as a reference frame.

We calculate the velocity gradient tensor from the calculated velocity field and use it as input into the D-Rex program (Kaminski et al., 2004). By applying molecular-scale physics to large-scale convection models, D-Rex allows us to track the LPO history in a flow field. The effects of intracrystalline slip and dynamic recrystallisation mechanisms are accounted for (Lassak et al., 2006). The projection method of Browaeys and Chevrot (2004) converts the output and gives the predicted magnitude of S-wave anisotropy and olivine's a -axis orientation at each node on a 36×20 grid (grid spacing of 40 km). This is much coarser than the finite element model as we are interested in the larger-scale flow field associated with the subducting slab. This grid spacing is similar to previous work on LPO modelling in subduction zones using the D-Rex method (e.g. Lassak et al., 2006).

First, we investigate the sensitivity of our LPO models to ranges of values in several different subduction zone parameters: model run time (5–25 Ma), oceanic lithosphere thickness (60–100 km) and slab rollback velocity (0–20 mm yr⁻¹). We investigate the effect of trench rollback as this is believed to exert a strong control on regional mantle flow beneath the Andean margin (Russo and Silver, 1994; Helffrich et al., 2002).

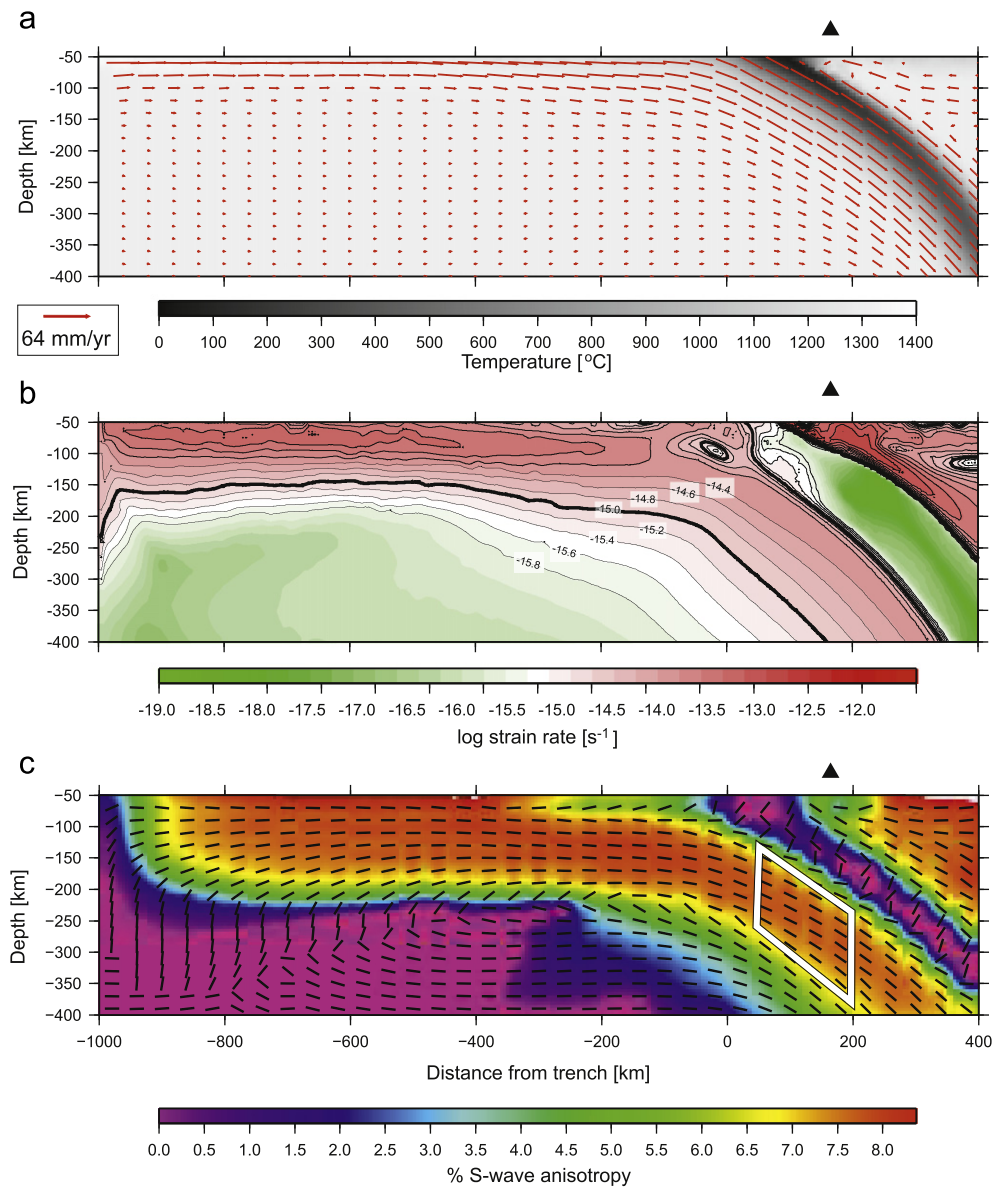


Fig. 5. Characteristics of our preferred numerical geodynamic model. (a) Temperature and velocity field. (b) Strain rate. (c) Predicted LPO: the colour represents magnitude of S-wave anisotropy and the orientation of the bars indicate the orientation of olivine's a -axis. The white box shows the approximate region of the sub-slab asthenosphere through which SKS rays traverse. The black triangle represents the approximate location of the TIPTEQ seismic network.

Since there is no observational evidence for the thickness of the Nazca lithosphere in this region, we centre our sensitivity tests on the value of 80 km given by Kawakatsu et al. (2009) for Japan. Our tests show that the strain rate field and LPO orientation in the sub-slab asthenosphere are dependent on the oceanic lithosphere thickness and slab rollback velocity. The highest strain rate ($\log \dot{\epsilon}_t \geq -14.2 \text{ s}^{-1}$), strongest S-wave anisotropy (7.7%) and coherent a -axis orientations in the sub-slab asthenosphere (plunging parallel to the dip of the slab) are generated using zero trench rollback and a thin (e.g. ≤ 80 km) and therefore young, oceanic lithosphere. We also find that long model run times, such as 25 Ma produce the largest area of high strain rate and most coherent a -axis orientations in the sub-slab asthenosphere.

We derive the best geodynamic model for the south-central Chile subduction zone by constraining the model parameters with evidence from the literature. Since the model run time is the first-order constraint on the slab geometry at depth, we require additional constraints on this. Seismicity (e.g. Bohm et al., 2002; Haberland et al., 2006) and receiver functions (Asch et al., 2006)

constrain the geometry of the downgoing Nazca slab to 115 km depth. Below this depth, however, global tomography models provide the only constraints on the slab's geometry at depth. The tomographic models of Becker and Boschi (2002) and Obayashi et al. (2009) indicate a degree of ponding of the Nazca slab in the mantle transition zone; we therefore let the model run for 15 Ma in order to allow the slab to pond in these depth ranges. Although trench rollback values can heavily depend on the reference frame used, we use a trench rollback velocity of 11 mm yr^{-1} (Lallemand et al., 2008) in the SB04 hotspot reference frame (Steinberger et al., 2004). We also employ an oceanic lithosphere of 45 km thickness predicted by the heat flow model of Stein and Stein (1992) for a 30 Ma old lithosphere (e.g. Tebbens and Cande, 1997; Müller et al., 2008).

Using the parameters above, our preferred model (Fig. 5) predicts values of strain rate and percentage of S-wave anisotropy in the supra-slab mantle wedge of a similar magnitude to those given by previous geodynamic modelling studies (Billen and Hirth, 2007; Kneller et al., 2008). Our model also shows a 150 km thick

layer of high strain rate in the sub-slab asthenosphere. The LPO model predicts this region to be strongly anisotropic (7.7% S-wave anisotropy); this value is similar to other studies which model the magnitude of S-wave anisotropy in the upper mantle (e.g. Becker et al., 2006; Nippres et al., 2007). We find that all SKS rays cross the region of the sub-slab asthenosphere with olivine a -axes plunging parallel to the dip of the slab ($\sim 35^\circ$), but do not traverse the region of high strain rate and strong anisotropy in the supra-slab asthenosphere.

5.2. Synthetic shear-wave splitting

To understand the splitting observations in more detail, it is important to forward model the measurements. This was done using SynthSplit, an open-source MATLAB code; it predicts shear-wave splitting parameters using the particle motion perturbation method of Fischer et al. (2000) and has been tested with full synthetic waveform methods (Abt and Fischer, 2006). SynthSplit requires input parameters which describe the anisotropic characteristics of each layer, the elastic parameters and the incoming ray's geometry. The method assumes single crystal anisotropic strength, but in the real Earth, anisotropy is much weaker than this; to account for this, we calculate a dilution factor using the following equation:

$$\% \text{ Dilution} = \frac{\% \text{ Natural S-wave anisotropy}}{\% \text{ Single crystal anisotropy}} \quad (1)$$

Using olivine's single crystal S-wave anisotropic strength of 18.1% (Kumazawa and Anderson, 1969) and the S-wave anisotropy magnitude strength in the sub-slab asthenosphere given by our LPO prediction model of 7.7%, we calculate a dilution factor of 42.5%. All models use a composition of 70%/30% olivine to orthopyroxene with orthorhombic symmetry.

To understand our first-order splitting pattern, we firstly attempt to model the mean NE teleseismic fast direction and

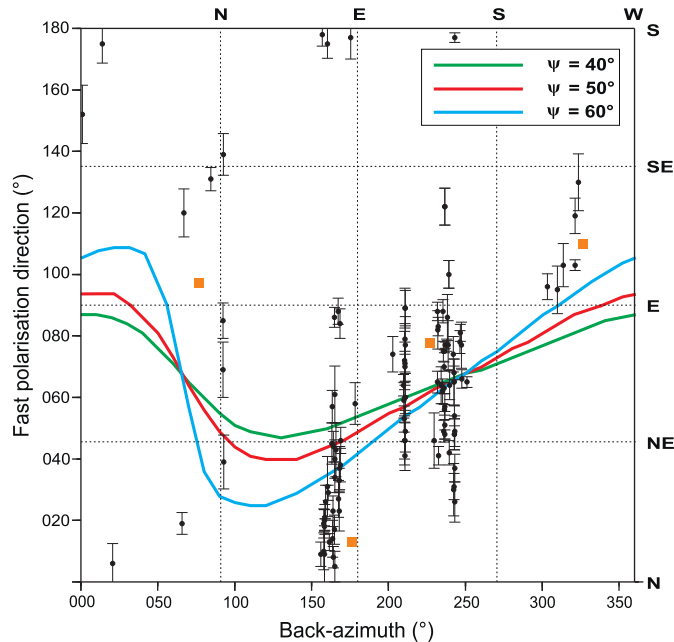


Fig. 6. Forward modelling the fast polarisation direction dependence on back-azimuth. Black circles are observed fast polarisation directions from the teleseismic shear-wave splitting measurements. The orange squares represent the stacked splitting measurements for each main back-azimuth cluster. The coloured lines represent the forward modelled back-azimuth - fast direction relationship, for different a -axis dip angles, ψ . The modelled fast polarisation directions were derived using an incidence angle of 15° and an a -axis azimuth of 067° , the absolute plate motion direction of the Nazca plate.

the teleseismic-local delay time residual of 1.1 s. Assuming a one-layer case, a horizontal olivine a -axis and a vertically incident ray, we find that a 140 km thick layer with an olivine a -axis azimuth parallel to the direction of the APM of the Nazca slab explains these residual splitting parameters.

We also investigate the possibility of two layers with different anisotropic characteristics causing the observed splitting. For any arbitrary two-layered model, delay time has a $\pi/2$ cyclicity with respect to back-azimuth (Savage and Silver, 1993). By incorporating another layer into the model described above, we are not able to increase the fit to our observed splitting parameters. Forward modelling using multiple layers is complex because for each layer, the number of parameters required to be input increases by five, so this is not a reasonable approach without additional constraints.

Finally, to explain the fast direction dependency on back-azimuth, we investigate the presence of a plunging olivine a -axis, as suggested by our geodynamic models. A model which uses a 140-km thick layer (derived from the strain rate and LPO models) with a moderately-dipping olivine a -axis (50 – 60°), parallel to the APM of the Nazca plate (067°) fits the fast direction data reasonably well (Fig. 6). This is somewhat steeper than the inferred 30° dip of the Nazca slab in this region (e.g. Haberland et al., 2006). For the incoming ray geometry, we use a constant incidence angle of 15° for all back-azimuths, this value is our calculated incidence angle from our SKS raypaths in the sub-slab asthenosphere (Fig. 2b). We find that the model reproduces well the range of measured SKS delay times.

6. Discussion

6.1. Comparisons with the regional shear-wave splitting framework

The average north-easterly SKS splitting directions in our study do not correlate with the overall trench-parallel teleseismic splitting directions observed along the western margin of South America (e.g. Russo and Silver, 1994; Bock et al., 1998; Rokosky et al., 2006; Long and Silver, 2008).

Regionally, trench-parallel observations by Russo et al. (2010) north of the Patagonian slab window do not match well with our results. Our fast directions derived from westerly back-azimuth events correlate with the ENE fast directions observed at station PLCA by Helffrich et al. (2002) and MacDougall et al. (2010). Similarly, our NNW fast directions from rays with a southerly back-azimuth compare better with the trench parallel fast directions further north (Anderson et al., 2006). A back-azimuthal dependence on splitting parameters is not seen at stations PLCA and TRQA, which are located further toward the back-arc (MacDougall, personal communication, 2011).

If the fast directions from station PLCA (Helffrich et al., 2002; MacDougall et al., 2010) are compared with those at the southern end of the CHARGE network (Anderson et al., 2006; MacDougall et al., 2010), and assuming these directions are not the subject of a back-azimuthal dependence, then somewhere in the south-central Chile forearc, a rotation in fast directions must exist, from trench-oblique in the south to trench-perpendicular in the north. If, however, a back-azimuthal dependency is a common regional feature, as it has been observed at some stations in central Chile (Anderson et al., 2006), and is not accounted for, then mantle flow directions could be misinterpreted.

6.2. Origin of the teleseismic fast direction dependency on back-azimuth

Back-azimuthal dependencies have been documented in a variety of locations, e.g. Tibet (McNamara et al., 1994) and the

Canadian shield (Bastow et al., 2011). For subduction zones, it appears to be a feature of shear-wave splitting in Cascadia (Hartog and Schwartz, 2000; Currie et al., 2004; Long et al., 2009; Russo, 2009; Rieger and Park, 2010), Alaska (Christensen and Abers, 2010), Sumatra (Collings et al., submitted for publication) and central Chile (Anderson et al., 2006). This pattern tends to be observable at stations close to the subduction trench and is associated with regions where relatively young oceanic lithosphere is subducted.

There are three explanations for this phenomenon. The most intuitive reason is that rays with different paths do not sample the same regions, so a heterogeneous shear-wave splitting pattern is observed at the surface. This has been used to explain the fast direction variation with back-azimuth in Alaska, because rays from only one direction sampled the supra-slab asthenospheric wedge (Christensen and Abers, 2010). Our teleseismic raytracing shows that the rays do not converge until they arrive at a depth of around 250 km. The raypaths and slab geometry in this study (Fig. 2b) show that the mid-lower mantle crossed by SKS rays is unlikely to be influenced by subduction of the Nazca slab; therefore it is unlikely to develop significant seismic anisotropy due to slab-induced deformation (e.g. Nippres et al., 2004; Foley and Long, 2011). Furthermore, where the rays converge, we would expect the SKS Fresnel zone radius to be around 60 km (e.g. Niu and Perez, 2004).

A dependence on back-azimuth may also be caused by multiple anisotropic layers. When two or more significantly strong and/or thick layers with distinct symmetry axes are present, the fast polarisation direction will have a $\pi/2$ cyclicity (Savage and Silver, 1993). Russo (2009) used this to explain source-side shear-wave splitting beneath Cascadia, caused by two layers of sub-slab asthenosphere, with perpendicular flow directions. We do not observe any periodicity in delay time as a function of back-azimuth and our splitting measurements are not easily explained by a model comprising two layers, although if one or more of these layers contains inclined symmetry axes, a straightforward $\pi/2$ periodicity would not be present (Brechner et al., 1998).

Finally, the existence of a plunging axis of symmetry (in this case, olivine's *a*-axis) in a layer of strongly anisotropic asthenosphere beneath the subducting slab has been used by Hartog and Schwartz (2000) and Collings et al. (submitted for publication) to explain a fast direction dependence on back-azimuth in the Cascadia and Sumatra subduction zones, respectively. Our LPO model shows that this mechanism could explain the observed back-azimuthal dependence in fast direction.

6.3. Anisotropic sources and potential mechanisms

Determining the depth to the primary source of anisotropy is complex; this is particularly true in subduction zones where there are a number of possible distinct source regions: continental crust, continental mantle, oceanic crust, oceanic lithospheric mantle and sub-slab asthenosphere. To interpret our splitting results, we consider all parts of the subduction system, the potential sources of anisotropy in each, and whether or not they have a strong signal in our splitting measurements.

6.3.1. Overriding continental lithosphere

Cracks and microcracks are the strongest sources of anisotropy found to be in upper crustal layers (Crampin, 1994). Ozalaybey and Savage (1995) found that shear-wave splitting measurements at stations close to the San Andreas fault record fast directions parallel to the strike of the fault. Away from the fault, it appears that crustal fast directions align with the direction of maximum horizontal compressive stress (e.g. Crampin et al., 2004; Huang et al., 2011).

The magnitude of our local shear-wave splitting delay times and their weak correlation with path length through the continental crust is consistent with a heterogeneous crustal source of anisotropy. The relative coherency of station stacks with respect to source stacks suggests that most local S-wave splitting is sourced in the upper, rather than lower crust. Upper crustal sources are likely to be important along the south-central Chile forearc due to active tectonics and related crustal faults. The average E–W fast direction of the station stacks is consistent with observations of maximum horizontal compressive stress directions, σ_H in the region (Heidbach et al., 2008). The apparent alignment of some fast directions with mapped fault traces is consistent with a SPO source in crustal fault zones.

The forearc mantle wedge is likely to be subject to both viscous and thermal erosion by asthenospheric wedge flow, resulting in a cold nose (Conder et al., 2002); these conditions are non-conducive to the preservation of LPO caused by coherent mantle flow. It is possible that anisotropy can be 'frozen-in' to the continental mantle, recording past plate motions (e.g. Long and van der Hilst, 2006). We observe no correlation between path length through the continental mantle and delay time; furthermore, our SKS rays arriving east of 72.5°W sample continental mantle, but we observe no east–west change in splitting parameters. We therefore reject the possibility of a strong source of anisotropy in the continental mantle.

It is clear that the overriding South American lithosphere contributes only a small amount (~ 0.2 s) to the total SKS splitting. We therefore focus on the slab, and the underlying mantle, as the main source SKS splitting must lie here. This is also emphasised by the delay times observed on Isla Mocha; here the overlying crust is no more than 15 km thick (Haberland et al., 2009); yet the SKS delay times are still in excess of 1 s. Since the overlap between the teleseismic and local frequency bands is limited, we filter 10 of our best SKS splits at the same frequency band as the local data (0.1–1.0 Hz). We find that the average SKS delay time in this frequency band is 0.88 s, over four times greater than the average local S delay time, but 0.5 s smaller than the SKS splitting average at lower frequency bands. Therefore, this indicates the strength of anisotropy varies with depth — the main source of SKS splitting must be sourced from beneath the subducting oceanic crust. SKS fast directions do not conclusively show frequency dependence, possibly indicating that anisotropy in the shallower and deeper layers may have a similar orientation (Wirth and Long, 2010).

6.3.2. Subducting oceanic lithosphere

Both Faccenda et al. (2008) and Healy et al. (2009) suggest that significant trench-parallel splitting can be caused by faults in the downgoing oceanic crust. Although clear signatures of these faults and associated serpentinisation are detected offshore (Contreras-Reyes et al., 2007), we do not observe consistent trench-parallel splitting. Raytracing of local S-waves shows that path lengths through the slab are not proportional to the observed delay time; therefore, the subducting oceanic crust in this region is not strongly anisotropic. For these reasons, we reject the hypothesis that the primary splitting signal is sourced in the downgoing oceanic crust.

In some recent shear-wave splitting studies, it has become common practice to attribute any strong teleseismic splitting unexplained by supra-slab anisotropy to fossil anisotropy in the downgoing oceanic mantle (e.g. Hammond et al., 2010; Christensen and Abers, 2010) caused by fossil anisotropy. In this case, the measured fast directions will be parallel to the oceanic lithosphere's APM. Although the interpreted teleseismic fast direction in our study is close to the Nazca plate's APM, its young age at the trench means the Nazca lithosphere should be 45 km

thick based on the model of Stein and Stein (1992). By subtracting the 8 km crustal layer from the lithosphere, we predict a 37 km thick oceanic mantle. We use the synthetic shear-wave splitting described above to determine whether the oceanic mantle can produce the observed delay time of more than 1 s. Assuming a vertically incident ray and a horizontal layer, we find that the oceanic mantle would need to have a natural S-wave anisotropy in excess of 20%. We believe that this magnitude of anisotropy is unreasonable, so we rule out a significant contribution to the teleseismic splitting from the oceanic mantle.

6.3.3. Sub-slab asthenosphere

The high teleseismic splitting delay times, compared to those of local splitting, and the lack of evidence for a strong source in the oceanic lithosphere suggest that most anisotropy is sourced from beneath the subducting Nazca slab.

Our geodynamic model predicts high strain rates in the sub-slab asthenosphere (Fig. 5); this characteristic is similar to the rheology-based model of Billen and Hirth (2007). High strain rates are conducive to dislocation creep, important for producing seismic anisotropy. Without accounting for the effect of grain size changes, Billen and Hirth (2007) find that at 250 km depth in the mantle, the transitional strain rate, $\dot{\epsilon}_t$, between dislocation and diffusion creep is $\log \dot{\epsilon}_t = -15 \text{ s}^{-1}$; strain rates above this value will promote dislocation creep, and subsequently, LPO formation/preservation. Our model comprises of a thick (150 km) layer with $\log \dot{\epsilon}_t \geq -15 \text{ s}^{-1}$ and strong (7.5–8.0%) shear-wave anisotropy; this value is within the range of shear-wave anisotropy from mantle-derived xenoliths (Ismail and Mainprice, 1998). Furthermore, the younger, and therefore, warmer Nazca lithosphere is likely to result in a warmer asthenosphere in the vicinity of the slab; this, along with the elevated strain rates will be more conducive to the predominance of dislocation creep in the sub-slab asthenosphere. These factors will promote the formation of significant LPO.

The back-azimuthal dependence on fast direction is modelled with a plunging olivine *a*-axis in the sub-slab asthenosphere; this is consistent with the mechanism of entrainment of the asthenosphere by the motion of the subducting Nazca slab. Slab-entrained asthenosphere was first discussed by Savage (1999), who predicted that a subducting slab should entrain the surrounding asthenosphere, causing a subduction-parallel, dipping symmetry axis. This idea has been neglected recently because of numerous global observations of trench-parallel fast directions, due to sub-slab barrier flow (Long and Silver, 2008). Phipps Morgan et al. (2007) recently modelled slab entrained flow; their numerical models predict that an entrained layer's thickness depends on subduction rate, and their analogue experiments predict that the layer will be thickest beneath the forearc, with a decreasing thickness toward the back-arc. This corresponds to the thickness of our forward-modelled layer from our data on the forearc and the lack of observational evidence for a back-azimuthal dependency in the back-arc region (MacDougall, personal communication, 2011).

Long and Silver (2009) made a link between the sub-slab entrainment model and observations of strong trench-perpendicular fast directions in Cascadia. They propose that shear heating occurs at the base of warmer lithosphere. Evidence for a sharp S-wave velocity decrease at the lithosphere–asthenosphere boundary (e.g. Kawakatsu et al., 2009) is explained by the presence of shear-heating derived partial melt (Long and Silver, 2009). Our inference of an entrained layer of asthenosphere beneath the slab, with symmetry axes parallel to the direction of the Nazca plate's APM, implies that the oceanic lithosphere and underlying asthenosphere are strongly coupled beneath south-central Chile.

We now associate south-central Chile with those subduction zones which are inferred to comprise significant sub-slab splitting

oriented in the direction of subduction. These include the Cascadia (Hartog and Schwartz, 2000; Currie et al., 2004; Russo, 2009; Rieger and Park, 2010), Rivera-Cocos (Soto et al., 2009), Alaska (Christensen and Abers, 2010) and the Sumatra (Hammond et al., 2010; Collings et al., submitted for publication) subduction zones. One characteristic that these regions share is the young age of the subducting lithosphere. Hammond et al. (2010) find a rotation toward subduction parallel teleseismic shear-wave splitting as the subducting lithosphere becomes progressively younger. This observation correlates well with the proposed model's relationship between lithospheric age and degree of shear heating. Where the lithosphere is younger and thinner, the shear heating mechanism will not have reached steady state (Long and Silver, 2009), so the lithosphere and asthenosphere will be more strongly coupled, leading to entrainment of sub-slab asthenosphere in the direction of subduction. Some of these studies describe observations showing a fast direction—back-azimuth relationship; these are from stations located on the forearc, close to the trench. At these stations, the strongest anisotropic signal is likely derived from the sub-slab asthenosphere since the SKS rays do not sample the supra-slab asthenospheric wedge. Whilst frozen-in anisotropy in the subducting lithospheric mantle is not disputed, the APM will also be expressed in the sub-slab asthenosphere.

We believe the fast directions observations will never perfectly fit a synthetically modelled fast direction—back-azimuth relationship. The real measurements may be complicated by return flow in the asthenosphere (Phipps Morgan et al., 2007) and it is possible that olivine's *a*-axis does not plunge at a constant angle throughout the entrained layer of asthenosphere. Furthermore, our forward modelling technique uses constant incidence angles and assumes that the thickness of the layer does not change laterally. For a 150 km thick layer dipping at 30°, we calculate that rays arriving from the down-dip direction will have a path length 50 km longer than those that arrive from the up-dip direction. The simplicity of our model means we do not account for these variable path lengths; this could partly explain the poor fit between the observed and modelled back-azimuth—splitting parameter relationships. We believe that scattered fast directions for each back-azimuth bin may be partly due to small differences between the back-azimuth and calculated initial polarisation direction (Fig. S7). These discrepancies may arise from the misalignment of station horizontal components (Evans et al., 2006). We also do not completely reject the case of a multi-layered flow; it may be possible that locally, we have entrained flow beneath the slab, and a larger scale regional trench-parallel flow beneath this, although our back-azimuthal coverage makes this a difficult hypothesis to test. We note the discrepancy between the modelled olivine *a*-axis dip and the actual dip of the Nazca slab; this could be a result of the simplified modelling described above. Physically, this difference could result from the fact that seismic anisotropy is an integrated effect of the strain history imposed by mantle flow, so there could be a signature of past subduction geometries in the observed shear-wave splitting.

7. Conclusions

Using data from a dense seismic network located on south-central Chilean forearc, we have used both teleseismic and local shear-wave splitting observations to improve our understanding of the region's anisotropic sources and their location, relative to the downgoing Nazca slab. Reconciling these observations with both geodynamic and synthetic forward models, we can further constrain the location and mechanism of the main anisotropic signal.

Small magnitude splitting measurements from local S-waves indicate comparatively weak anisotropic sources associated with an upper crustal source of anisotropy. We observe significant splitting of teleseismic SKS arrivals; their average delay time is seven times greater than that from local splitting. A significant source of

anisotropy, therefore, lies either within or below the Nazca slab. Both our geodynamic models and our synthetic shear-wave splitting analysis point towards the presence of strongly anisotropic sub-slab asthenosphere comprising olivine a -axes oriented parallel to the horizontal APM, and dip angle of the subducting Nazca slab. We explain these observations with a model of sub-slab asthenosphere being entrained by the motion of the downgoing Nazca slab. This mechanism's signal in the shear-wave splitting appears to be clearest when measured on the forearc, where the slab is shallowest and no supra-slab asthenospheric wedge is present.

We have provided evidence for a new mechanism to explain shear-wave splitting along the Andean margin of South America. We have shown that the inferred anisotropy beneath this region can be explained by a model comprising a thick layer of sub-slab entrained asthenosphere, with little contribution from the other subduction domains. This model infers strong coupling between the Nazca lithosphere and the underlying stable mantle. We have shown that this model can be applied to forearc observations of shear-wave splitting in several other young subduction zones. The model of Long and Silver (2008) compiled from global observations of shear-wave splitting requires a thin decoupling zone between the downgoing slab and the sub-slab asthenosphere because significant anisotropic signals from slab-entrained flow are not commonplace. However, we can now group the south-central Chile subduction zone with the Cascadian margin as regions which prove exceptions to this global model (Long and Silver, 2008).

Our model could have important implications for both the nature of sub-slab asthenosphere and the lithosphere–asthenosphere boundary. If buoyant asthenosphere is upwelled beneath hotspots, asthenosphere is likely to be returned to the deeper mantle through subduction processes. Furthermore, this sub-slab asthenospheric layer with a non-Newtonian rheology will have a considerably lower effective viscosity; the presence of such a layer beneath a slab could control how slabs descend through the upper mantle. Finally, if this weak layer is present below the oceanic lithosphere prior to subduction, it could facilitate subduction initiation by decreasing the hydrodynamic stresses on the slab (Billen and Hirth, 2005).

Acknowledgments

We thank two anonymous reviewers for their constructive and insightful comments. We are grateful to Matthew Whipple for carrying out some of the preliminary data analysis, and Rachel Collings for assistance with the local raytracing. Dr. David Abt made his codes for calculating shear-wave splitting freely available and provided some related assistance. We would like to thank all members of the TIPTAQ fieldwork group and the landowners of south-central Chile. Seismic instruments were provided by GIPP (GFZ). Figures were created using the GMT software package (Wessel and Smith, 1998) and seismic processing was done with SAC (Seismic Analysis Code).

Appendix A. Supplementary data

Supplementary data associated with this article can be found in the online version at <http://dx.doi.org/10.1016/j.epsl.2012.09.017>.

References

- Abt, D., Fischer, K., 2008. Resolving three-dimensional anisotropic structure with shear wave splitting tomography. *Geophys. J. Int.* 173 (3), 859–886.
- Anderson, M., Zandt, G., Triep, E., Fouch, M., Beck, S., 2004. Anisotropy and mantle flow in the Chile–Argentina subduction zone from shear wave splitting analysis. *Geophys. Res. Lett.* 31 (23), L23608.
- Angermann, D., Klotz, J., Reigber, C., 1999. Space-geodetic estimation of the Nazca–South America Euler vector. *Earth Planet. Sci. Lett.* 171 (3), 329–334.
- Asch, G., Schurr, B., Bohm, M., Yuan, X., Haberland, C., Heit, B., Kind, R., Woelbern, I., Bataille, K., Comte, D., et al., 2006. Seismological studies of the Central and Southern Andes. *The Andes*, 443–457.
- Bastow, I., Thompson, D., Wookey, J., Kendall, J., et al., 2011. Precambrian plate tectonics: seismic evidence from northern Hudson Bay, Canada. *Geology* 39 (1), 91.
- Becker, T., Boschi, L., 2002. A comparison of tomographic and geodynamic mantle models. *Geochem. Geophys. Geosyst.* 3, 1003.
- Becker, T., Chevrot, S., Schulte-Pelkum, V., Blackman, D., 2006. Statistical properties of seismic anisotropy predicted by upper mantle geodynamic models. *J. Geophys. Res.* 111 (B10), B08309.
- Billen, M., Hirth, G., 2005. Newtonian versus non-newtonian upper mantle viscosity: implications for subduction initiation. *Geophys. Res. Lett.* 32, 19304.
- Billen, M., Hirth, G., 2007. Rheologic controls on slab dynamics. *Geochem. Geophys. Geosyst.* 8, Q08012.
- Bock, G., Kind, R., Rudloff, A., Asch, G., 1998. Shear wave anisotropy in the upper mantle beneath the Nazca plate in northern Chile. *J. Geophys. Res.* 103 (B10), 24333.
- Bohm, M., Lüth, S., Echtler, H., Asch, G., Bataille, K., Bruhn, C., Rietbrock, A., Wigger, P., 2002. The southern andes between 36 and 40 s latitude: seismicity and average seismic velocities. *Tectonophysics* 356 (4), 275–289.
- Brechner, S., Klinge, K., Krüger, F., Plenefisch, T., 1998. Backazimuthal variations of splitting parameters of teleseismic SKS phases observed at the broadband stations in Germany. *Pure Appl. Geophys.* 151 (2), 305–332.
- Browaays, J., Chevrot, S., 2004. Decomposition of the elastic tensor and geophysical applications. *Geophys. J. Int.* 159 (2), 667–678.
- Christensen, D., Abers, G., 2010. Seismic anisotropy under central Alaska from SKS splitting observations. *J. Geophys. Res.* 115 (B4), B04315.
- Conder, J., Wiens, D., Morris, J., 2002. On the decompression melting structure at volcanic arcs and back-arc spreading centers. *Geophys. Res. Lett.* 29 (15), 1727.
- Collings, R., Lange, D., Tilmann, F., Nippres, S., Natawidjaja, D. Seismic anisotropy in the Sumatra subduction zone. *J. Geophys. Res.*, submitted for publication.
- Contreras-Reyes, E., Grevemeyer, I., Flueh, E., Scherwath, M., Heesemann, M., 2007. Alteration of the subducting oceanic lithosphere at the southern central Chile trench–outer rise. *Geochem. Geophys. Geosyst.* 8 (7), Q07003.
- Crampin, S., 1994. The fracture criticality of crustal rocks. *Geophys. J. Int.* 118 (2), 428–438.
- Crampin, S., Peacock, S., Gao, Y., Chastin, S., 2004. The scatter of time-delays in shear-wave splitting above small earthquakes. *Geophys. J. Int.* 156 (1), 39–44.
- Crotwell, H., Owens, T., Ritsema, J., 1999. The TauP Toolkit: flexible seismic travel-time and ray-path utilities. *Seismol. Res. Lett.* 70, 154–160.
- Currie, C., Cassidy, J., Hyndman, R., Bostock, M., 2004. Shear wave anisotropy beneath the Cascadia subduction zone and western North American craton. *Geophys. J. Int.* 157 (1), 341–353.
- Dabrowski, M., Krotkiewski, M., Schmid, D., 2008. MILAMIN: MATLAB-based finite element method solver for large problems. *Geochem. Geophys. Geosyst.* 9 (4), Q04030.
- Evans, M., Kendall, J., Willemann, R., 2006. Automated SKS splitting and upper-mantle anisotropy beneath canadian seismic stations. *Geophys. J. Int.* 165 (3), 931–942.
- Faccenda, M., Burlini, L., Gerya, T., Mainprice, D., 2008. Fault-induced seismic anisotropy by hydration in subducting oceanic plates. *Nature* 455 (7216), 1097–1100.
- Fischer, K., Parmentier, E., Stine, A., Wolf, E., 2000. Modeling anisotropy and plate-driven flow in the Tonga subduction zone back arc. *J. Geophys. Res.* 105 (B7), 16181.
- Foley, B., Long, M., 2011. Upper and mid-mantle anisotropy beneath the tonga slab. *Geophys. Res. Lett.* 38 (2), L02303.
- Fry, A., Kusznir, N., Rietbrock, A., Dabrowski, M., Podladchikov, Y., 2009. Modelling stress accumulation and dissipation in subducting lithosphere and the origins of double and triple seismic zones, In: AGU Fall Meeting Abstracts, vol. 1. p. 1917.
- Gripp, A., Gordon, R., 2002. Young tracks of hotspots and current plate velocities. *Geophys. J. Int.* 150 (2), 321–361.
- Groß, K., Micksch, U., 2008. The reflection seismic survey of project TIPTAQ—the inventory of the Chilean subduction zone at 38.2°S. *Geophys. J. Int.* 172 (2), 565–571.
- Haberland, C., Rietbrock, A., Lange, D., Bataille, K., Dahm, T., 2009. Structure of the seismogenic zone of the southcentral Chilean margin revealed by local earthquake traveltime tomography. *J. Geophys. Res.* 114 (B1), B01317.
- Haberland, C., Rietbrock, A., Lange, D., Bataille, K., Hofmann, S., 2006. Interaction between forearc and oceanic plate at the south-central Chilean margin as seen in local seismic data. *Geophys. Res. Lett.* 33 (23), L23302.
- Hammond, J., Wookey, J., Kaneshima, S., Inoue, H., Yamashina, T., Harjadi, P., 2010. Systematic variation in anisotropy beneath the mantle wedge in the Java–Sumatra subduction system from shear-wave splitting. *Phys. Earth Planet. Int.* 178 (3–4), 189–201.
- Hartog, R., Schwartz, S., 2000. Subduction-induced strain in the upper mantle east of the Mendocino triple junction, California. *J. Geophys. Res.* 105 (B4), 7909–7930.
- Hayes, G., Wald, D., 2009. Developing framework to constrain the geometry of the seismic rupture plane on subduction interfaces a priori—a probabilistic approach. *Geophys. J. Int.* 176 (3), 951–964.

- Healy, D., Reddy, S., Timms, N., Gray, E., Brovarone, A., 2009. Trench-parallel fast axes of seismic anisotropy due to fluid-filled cracks in subducting slabs. *Earth Planet. Sci. Lett.* 283 (1–4), 75–86.
- Heidbach, O., Tingay, M., Barth, A., Reinecker, J., Kurfeß, D., Müller, B., 2008. The World Stress Map database release 2008 <http://dx.doi.org/10.1594/GFZ.WSM.Rel2008>.
- Helfrich, G., Wiens, D., Vera, E., Barrientos, S., Shore, P., Robertson, S., Adaros, R., 2002. A teleseismic shear-wave splitting study to investigate mantle flow around South America and implications for plate-driving forces. *Geophys. J. Int.* 149 (1), F1–F7.
- Huang, Z., Zhao, D., Wang, L., 2011. Shear wave anisotropy in the crust, mantle wedge, and subducting Pacific slab under northeast Japan. *Geochem. Geophys. Geosyst.* 12 (1), Q01002.
- Ismaïl, W., Mainprice, D., 1998. An olivine fabric database: an overview of upper mantle fabrics and seismic anisotropy. *Tectonophysics* 296 (1–2), 145–157.
- Kaminski, E., Ribe, N., Browaeys, J., 2004. D-Rex, a program for calculation of seismic anisotropy due to crystal lattice preferred orientation in the convective upper mantle. *Geophys. J. Int.* 158 (2), 744–752.
- Karato, S., Jung, H., Katayama, I., Skemer, P., 2008. Geodynamic significance of seismic anisotropy of the upper mantle: new insights from laboratory studies. *Annu. Rev. Earth Planet. Sci.* 36 (1), 59.
- Kawakatsu, H., Kumar, P., Takei, Y., Shinohara, M., Kanazawa, T., Araki, E., Suyehiro, K., 2009. Seismic evidence for sharp lithosphere-asthenosphere boundaries of oceanic plates. *Science* 324 (5926), 499.
- Kennett, B., Engdahl, E., Buland, R., 1995. Constraints on seismic velocities in the Earth from traveltimes. *Geophys. J. Int.* 122 (1), 108–124.
- Kneller, E., Long, M., van Keken, P., 2008. Olivine fabric transitions and shear wave anisotropy in the ryukyu subduction system. *Earth Planet. Sci. Lett.* 268 (3), 268–282.
- Kneller, E., Van Keken, P., 2007. *Nature* 450 (7173), 1222–1225.
- Kneller, E., van Keken, P., 2008. Effect of three-dimensional slab geometry on deformation in the mantle wedge: implications for shear wave anisotropy. *Geochem. Geophys. Geosyst.* 9 (1), Q01003.
- Kumazawa, M., Anderson, O., 1969. Elastic moduli, pressure derivatives and temperature derivatives, of single-crystal olivine and single-crystal forsterite. *J. Geophys. Res.* 74 (25), 5961–5972.
- Lallemant, S., Heuret, A., Faccenna, C., Funicello, F., 2008. Subduction dynamics as revealed by trench migration. *Tectonics* 27 (3), TC3014.
- Lassak, T., Fouch, M., Hall, C., Kaminski, É., 2006. Seismic characterization of mantle flow in subduction systems: can we resolve a hydrated mantle wedge? *Earth Planet. Sci. Lett.* 243 (3–4), 632–649.
- Long, M., Gao, H., Klaus, A., Wagner, L., Fouch, M., James, D., Humphreys, E., 2009. Shear wave splitting and the pattern of mantle flow beneath eastern Oregon. *Earth Planet. Sci. Lett.* 288 (3–4), 359–369.
- Long, M., Silver, P., 2008. The subduction zone flow field from seismic anisotropy: a global view. *Science* 319 (5861), 315.
- Long, M., Silver, P., 2009. Mantle flow in subduction systems: the slab flow field and implications for mantle dynamics. *J. Geophys. Res.* 114 (B10), B10312.
- Long, M., van der Hilst, R., 2006. Shear wave splitting from local events beneath the Ryukyu arc: trench-parallel anisotropy in the mantle wedge. *Phys. Earth Planet. In.* 155 (3–4), 300–312.
- MacDougall, J., Fischer, K., Anderson, M., 2010. Shear-wave splitting and mantle anisotropy in the southern South American subduction zone. In: *AGU Fall Meeting Abstracts*, vol. 1. p. 2046.
- Mainprice, D., Tommasi, A., Couvy, H., Cordier, P., Frost, D., 2005. Pressure sensitivity of olivine slip systems and seismic anisotropy of earth's upper mantle. *Nature* 433 (7027), 731–733.
- McNamara, D., Owens, T., Silver, P., Wu, F., 1994. Shear wave anisotropy beneath the Tibetan Plateau. *J. Geophys. Res.* 99 (B7), 13655–13.
- Melnick, D., Bookhagen, B., Strecker, M., Echtler, H., 2009. Segmentation of megathrust rupture zones from fore-arc deformation patterns over hundreds to millions of years, Arauco peninsula, Chile. *J. Geophys. Res.* 114 (B1), B01407.
- Melnick, D., Echtler, H., 2006. Morphotectonic and geologic digital map compilations of the south-central Andes (36–42 S). *The Andes*, 565–568.
- Müller, R., Sdrolias, M., Gaiña, C., Roest, W., 2008. Age, spreading rates, and spreading asymmetry of the world's ocean crust. *Geochem. Geophys. Geosyst.* 9 (4), Q04006.
- Nippress, S., Kuszniir, N., Kendall, J., 2004. Modeling of lower mantle seismic anisotropy beneath subduction zones. *Geophys. Res. Lett.* 31 (19), L19612.
- Nippress, S., Kuszniir, N., Kendall, J., 2007. LPO predicted seismic anisotropy beneath a simple model of a mid-ocean ridge. *Geophys. Res. Lett.* 34 (14), L14309.
- Niu, F., Perez, A., 2004. Seismic anisotropy in the lower mantle: a comparison of waveform splitting of SKS and SKKS. *Geophys. Res. Lett.* 31 (24), L24612.
- Obayashi, M., Yoshimitsu, J., Fukao, Y., 2009. Tearing of stagnant slab. *Science* 324 (5931), 1173.
- Ozalaybey, S., Savage, M., 1995. Shear-wave splitting beneath western United States in relation to plate tectonics. *J. Geophys. Res.* 100 (B9), 18135–18.
- Peyton, V., Levin, V., Park, J., Brandon, M., Lees, J., Gordeev, E., Ozerov, A., 2001. Mantle flow at a slab edge: seismic anisotropy in the Kamchatka region. *Geophys. Res. Lett.* 28 (2), 379–382.
- Phipps Morgan, J., Hasenclever, J., Hort, M., Rüpke, L., Parmentier, E., 2007. On subducting slab entrainment of buoyant asthenosphere. *Terra Nova* 19 (3), 167–173.
- Polet, J., Silver, P., Beck, S., Wallace, T., Zandt, G., Ruppert, S., Kind, R., Rudloff, A., 2000. Shear wave anisotropy beneath the Andes from the BANJO, SEDA, and PISCO experiments. *J. Geophys. Res.* 105 (B3), 6287–6304.
- Restivo, A., Helfrich, G., 1999. Teleseismic shear wave splitting measurements in noisy environments. *Geophys. J. Int.* 137, 821–830.
- Richardson, R., Coblenz, D., 1994. Stress modeling in the andes: constraints on the south american intraplate stress magnitudes. *J. Geophys. Res.* 99 (B11), 22015–22022.
- Rieger, D., Park, J., 2010. USArray observations of quasi-Love surface wave scattering: orienting anisotropy in the Cascadia plate boundary. *J. Geophys. Res.* 115 (B5), B05306.
- Rietbrock, A., Haberland, C., Bataille, K., Dahm, T., Oncken, O., 2005. Studying the seismogenic coupling zone with a passive seismic array. *Eos Trans. AGU* 86 (32), 293.
- Rokosky, J., Lay, T., Garnero, E., 2006. Small-scale lateral variations in azimuthally anisotropic D"structure beneath the Cocos Plate. *Earth Planet. Sci. Lett.* 248 (1–2), 411–425.
- Russo, R., 2009. Subducted oceanic asthenosphere and upper mantle flow beneath the Juan de Fuca slab. *Lithosphere* 1 (4), 195.
- Russo, R., Gallego, A., Comte, D., Mocanu, V., Murdie, R., VanDecar, J., 2010. Source-side shear wave splitting and upper mantle flow in the Chile Ridge subduction region. *Geology* 38 (8), 707.
- Russo, R., Silver, P., 1994. Trench-Parallel flow beneath the Nazca plate from seismic anisotropy. *Science* 263 (5150), 1105.
- Savage, M., 1999. Seismic anisotropy and mantle deformation: what have we learned from shear wave splitting?. *Rev. Geophys.* 37 (1), 65–106.
- Savage, M., Silver, P., 1993. Mantle deformation and tectonics: constraints from seismic anisotropy in the western United States. *Phys. Earth Planet. In.* 78 (3–4), 207–227.
- Silver, P., Chan, W., 1991. Shear wave splitting and subcontinental mantle deformation. *J. Geophys. Res.* 96 (B10), 16429.
- Soto, G., Ni, J., Grand, S., Sandvol, E., Valenzuela, R., Speziale, M., González, J., Reyes, T., 2009. Mantle flow in the Rivera-Cocos subduction zone. *Geophys. J. Int.* 179 (2), 1004–1012.
- Stein, C., Stein, S., 1992. A model for the global variation in oceanic depth and heat flow with lithospheric age. *Nature* 359 (6391), 123–129.
- Steinberger, B., Sutherland, R., O'Connell, R., 2004. Prediction of emperor-hawaii seamount locations from a revised model of global plate motion and mantle flow. *Nature* 430 (6996), 167–173.
- Teanby, N., Kendall, J., Van der Baan, M., 2004. Automation of shear-wave splitting measurements using cluster analysis. *Bull. Seismol. Soc. Am.* 94 (2), 453.
- Tebbens, S., Cande, S., 1997. Southeast Pacific tectonic evolution from early Oligocene to present. *J. Geophys. Res.* 102 (B6), 12061–12.
- Wessel, P., Smith, W., 1998. New improved version of generic mapping tools released. *Eos. Trans. AGU* 79, 579.
- Wirth, E., Long, M.D., 2010. Frequency-dependent shear wave splitting beneath the Japan and Izu-Bonin subduction zones. *Phys. Earth Planet. Inter.* 181, 141–154.
- Wolfe, C., Silver, P., 1998. Seismic anisotropy of oceanic upper mantle: shear wave splitting methodologies and observations. *J. Geophys. Res.* 103 (B1), 749–771.